International Journal of Refrigeration
35 (2012) 1418 - 1429

Experimental study on condensation heat transfer and pressure drop of low GWP refrigerant HFO1234yf in a horizontal tube

Linlin Wang,* *Chaobin Dang,* *Eiji Hihara*

Institute of Environmental Studies, Graduate School of Frontier Sciences, The University of Tokyo, 5-1-5 Kashiwanoha, Kashiwa-shi, Chiba, 277-8563, Japan

*Corresponding author. E-mail: [wanglinlin@hee.k.u-tokyo.ac.jp] Tel./Fax: [+81 4 7136 4631]

Postal address: Environmental Studies Building #285, the University of Tokyo, 5-1-5 Kashiwanoha, Kashiwa, Chiba 277-8563, Japan

Abstract

Condensation heat transfer of low GWP refrigerant HFO1234yf was measured in a horizontal tube (inner diameter: 4 mm) at a mass flux range of 100 - 400 kg m^{-2} s^{-1} and different saturation temperatures (40, 45, and 50 ºC), and the results were compared with that of R134a, and R32. Effects of mass flux, vapor quality, saturation temperature, and thermophysical properties on the heat transfer coefficient were analyzed. Mass flux and vapor quality were presented to primarily affect the heat transfer coefficient in shear-force dominated flow regimes, whereas the thermal conductivity and density ratio are the primary parameters as thermophysical properties influencing the heat transfer coefficient. Observed annular flow regimes agreed with Tandon's flow pattern map. The measured pressure drop compared with that predicted by the Lockhart-Matinelli correlation, Huang correlation and Haraguchi correlation. And, when comparing the experimental heat transfer coefficient with four heat transfer coefficient correlations, the Haraguchi correlation fairly agreed with the experimental data, with a 10.8 % mean deviation.

Keywords: Condensation heat transfer, HFO1234yf, R134a, R32, Heat transfer characteristic, Flow pattern

1. Introduction

Increased attention to environmental problems has resulted in the evolution of refrigerants from chlorofluorocarbans (CFCs), and hydrochlorofluorocarbans (HCFCs), to hydrofluorocarbans (HFCs). Although HFC refrigerants have no ozone depletion potential (ODP), many of them have a relatively high global warming potential (GWP). For example, R134a, having a GWP of 1300, is being used extensively in automobile air conditioners (MACs). In order to reduce the environmental impact of MAC, HFO1234yf, with a GWP as low as 4, has been proposed as a promising alternative refrigerant applied in MAC.

Some works (Barbara, M.,Mark, S.,2008) (SAE, 2009) have been conducted to clarify the characteristics

of HFO1234yf as a refrigerant, including flammability, toxicity, environmental impact, thermodynamic properties; and material compatibility. However, few studies in the open literature have examined heat transfer characteristics in a condenser using HFO1234yf, which is essential in the design and optimization of HFO1234yf heat pump systems.

Many studies have proposed heat transfer models during condensation. Shah (1978) developed a condensation heat transfer correlation based on their saturated boiling heat transfer correlation by noting the similarity between the mechanisms of heat transfer during film condensation and boiling without bubble nucleation. This correlation is only applicable for annular flow. Dobson (1994) and Dobson and Chato (1998) experimentally studied the local heat transfer for in-tube condensation using R134a, R22, R12, and near-azeotropic refrigerant blend R32/R125 in a smooth copper tube with an inner diameter (ID) ranging from 3.14 mm to 7.04 mm. They developed two correlations based on the observed flow regimes for wavy flow and annular flow, respectively, and utilized the Froude number as the criterion to distinguish the transition of flow regimes. Soliman et al. (1971) and Soliman (1983, 1986) developed a theory for correlating the mist-annular transition during condensation based on a balance of destructive and stabilizing forces acting on the liquid film. On the basis of flow pattern observation, they proposed using the Froude number and a modified Weber number to define the change from wavy to annular flow and annular to mist flow, respectively. Haraguchi et al. (1994) experimentally studied the heat transfer coefficient and pressure drop during condensation using R22, R134a, and R123 in an 8.4 mm ID horizontal smooth tube. On the basis of the turbulent liquid film theory (Traviss et al., 1971) and Nusselt's theory, they proposed an empirical asymptotic equation with the power of 2 for predicting the local heat transfer coefficient. And, they also proposed a empirical expression for predicting the local frictional pressure drop. Cavallini et al. (2006) proposed a new simple method based on the flow pattern to determine the local heat transfer coefficient during condensation in horizontal smooth tubes with ID > 3 mm. The proposed correlation includes two equations for ΔT-independent and ΔT-dependent flow regions, respectively. Here, ΔT refers to the temperature difference between the saturation temperature and the wall temperature. In addition, Delcol et al., (2010) compared the condensation heat transfer experimental results using HFO1234yf with correlation of Cavallini et al. (2006). The study conducted by Delcol et al., (2010) is the only research available in open literature on the condensation heat transfer of HFO1234yf. Recently, Saitoh et al. (2011) published experimental results of the flow boiling heat transfer coefficient of HFO1234yf inside a smooth small-diameter horizontal tube, and demonstrated that the boiling heat transfer coefficient of HFO1234yf is approximately similar to that of R134a. Huang(2010) experimentally investigated the two-phase friction pressure drop characteristics of R410A-oil mixture flow condensation inside 4.18mm and 1.6mm I.D. horizontal smooth tubes. And based on the experimental results, they proposed a new correlation for the frictional pressure drop.

In the present research, condensation heat transfer characteristics of HFO1234yf were experimentally studies, and the results were compared to those of R134a and R32. The effects of various parameters, including mass flux, vapor quality, saturation temperature and thermophysical properties on the condensation heat transfer performance were discussed.

2. Experimental Apparatus

Figure 1 shows a schematic of the experimental apparatus. The refrigerant loop comprises a test section, two sight glasses, a post-condenser, an accumulator, an expansion valve, a filter, a liquid pump, a mass flow meter, an evaporator, and three water baths. The saturation temperature and pressure of the test section is controlled by the opening of the expansion valve, and the water baths are used to adjust the inlet superheating of test section, provide cooling water to test section, and subcool the refrigerant flowing out of the test section, respectively.

Figure 2 is a detailed diagram of the test sub-sections. The test condensation tube is made of copper with an inner diameter of 4 mm and an overall length of 3.4 m. It is divided into five sub-sections; with each sub-section has an effective length of 0.45 m. All the sub-sections were cooled separately by the cooling water and the average condensation heat transfer coefficient of each sub-section was measured. The refrigerant flows inside the copper tube, and the cooling water flows in reverse direction within annular region between the inner tube and outer tube. For each sub-section, the mass flow rate of the cooling water was controlled independently. In order to make average heat flux in each sub-section is almost same, the inlet temperature and mass flow rate of cooling water were controlled. The inlet and outlet temperatures of the cooling water were measured using platinum resistance thermometers. Nine T-type thermocouples were soldered at the outer surface of copper tube with an interval of 12.5 cm between thermocouples. To reduce the heat loss to the surroundings, the entire apparatus including the refrigerant loop and the coolant loop was heavily insulated.

The cooling water loop includes a re-circulating chiller, mass flow meters, filters, and flow rate controlling valves. The re-circulating chiller provides cooling water for each sub-section at the desired temperature. The temperatures at the inlet and outlet of each sub-section were measured using platinum resistance sensers. The cooling water flow rate of each sub-section was measured using a positive displacement flow meter attached to that path.

All the temperature sensors, including the thermocouples and platinum resistance sensors, were calibrated by using a high precision resistance thermometer (Chino, Model F201-A-2) with an accuracy of ±0.01ºC. The accuracy of the calibrated thermocouples was within ±0.1ºC, and the calibrated platinum resistance sensors were within ±0.05ºC. The mass flow rate on the refrigerant side was measured by a Coriolis-type mass flow meter with an accuracy of ±0.1%. The mass flow rates of the cooling water were measured by positive displacement flow meters with an accuracy of ±1.0%. Pressures changing inside the test section were measured using an ultra precision digiquartz manometer (Sokken, Model 660) with an accuracy of ±1.0 kPa. The flow patterns inside the sight glass were observed and recorded using a high-speed digital camera (Photron, Fastcam SA4). Besides, the accuracy of the length of the test sections was within ±1.0 mm, and the diameter of the tube was within ±0.1 mm.

3. Data Reduction

The average heat transfer coefficient h_{exp} of each sub-section was determined by calculating the ratio of the average heat flux q to the temperature difference between saturation temperature T_s and inner wall

temperature T_{wall}, as follows:

$$h_{exp} = \frac{q}{T_s - T_{wall}} \quad (1)$$

The average heat flux q was determined from the heat exchange rate Q at the cooling water side by using the inlet and outlet temperatures (T_{in}, T_{out}) and the mass flow rate m_w:

$$Q = c_p m_w (T_{out} - T_{in}) \quad (2)$$

$$q = \frac{Q}{\pi d l} \quad (3)$$

The inner wall temperature T_{wall} of the copper tube was derived from the measured outer wall temperature T_{wo} and the heat exchange rate Q:

$$T_{wi}(x) = T_{wo}(x) + Q_i(x) \frac{\ln(d_o / d)}{2\pi k l} \quad (4)$$

The saturation temperature was calculated from the corresponding saturation pressure. The refrigerant side pressures were measured at three locations along the entire condensation tube. The pressure at the inlet and outlet of each sub-section was calculated by linearly interpolating the measured values.

4. Results and Discussion

4.1 Heat transfer characteristics of HFO1234yf

4.1.1 Uncertainty of the heat transfer coefficients

Figure 3 shows examples of the measured heat transfer coefficients of HFO1234yf at a saturation temperature of 45 ºC with the mass fluxes ranging from 100 kg m^{-2} $s^{-1}$to 400 kg m^{-2} s^{-1}. The measurement uncertainty of the heat transfer coefficient is illustrated using a vertical error bar for each experimental data. In general, the first measured point near the condenser entrance has the largest measurement uncertainty because the temperature difference between the saturation temperature and wall temperature is small. At a mass flux of 100 kg m^{-2} s^{-1}, the first point may have an uncertainty of up to 21%. The average measurement uncertainty of the heat transfer coefficient at this mass flux is 14%. At mass fluxes ranging from 200 kg m^{-2} s^{-1} to 400 kg m^{-2} s^{-1}, the measurement uncertainty of the heat transfer coefficient is relatively small, mostly below 10%, and has an average value of 7.8%. The measurement uncertainties in the case of other pure refrigerants and other saturation temperatures have similar trends and values.

4.1.2 Effects of mass flux and vapor quality

Figure 3 also shows the effects of mass flux and vapor quality on the heat transfer coefficient of HFO1234yf at a saturation temperature of 45 ºC. The heat transfer coefficient increases with an increase in mass flux and vapor quality, especially when the mass flux is larger than 200 kg m^{-2} s^{-1}. At annular flow regimes (force convection condensation in shear dominated flow regimes), the heat transfer coefficient is primarily influenced by the mass flux and vapor quality. The difference in the heat transfer coefficient for mass fluxes ranging between 100 kg m^{-2} s^{-1} and 200 kg m^{-2} s^{-1} is small because the flow patterns are primarily gravity-dominated flow regimes. As demonstrated by Dobson and Chato (1998), during condensation, the heat transfer mechanism can be divided into three parts: shear-dominated flow regime, gravity-dominated flow regime and an intermediate flow region. In shear-dominated flow regime, the local heat transfer coefficient is primarily affected by the mass flux and vapor quality. In contrast, in the gravity-dominated flow regime, the local heat transfer coefficient is mainly affected by the temperature

difference between the wall and bulk refrigerant. Whereas for intermediate flow regime, both the above mentioned heat transfer mechanisms exist in the heat transfer process. At mass fluxes of 100 kg m^{-2} s^{-1} and 200 kg m^{-2} s^{-1}, when vapor quality were less than 0.5, the difference of the heat transfer coefficients is small at these two mass flux, and the vapor quality change little, which means that the mass flux and vapor quality have little influence on heat transfer coefficient. This is especially the case when the heat transfer is entirely in the gravity- dominated flow regimes where the main thermal resistance is film thickness for heat transfer.

4.1.3 Effects of saturation temperature

Figure 4 shows the effect of the saturation temperature on the heat transfer coefficient of HFO1234yf at saturation temperatures of 40 ºC and 50 ºC, with mass fluxes ranging from 100 kg m^{-2} s^{-1} to 400 kg m^{-2} s^{-1}. The heat transfer coefficient was found to decreases slightly at same mass fluxes as the saturation temperature increased. Table1 shows the thermodynamic properties of HFO1234yf at the saturation temperature of 40 ºC and 50 ºC. At a saturation temperature of 40 ºC, the liquid/gas density ratio is 17.9, and thermal conductivity of the liquid is 63.0 mW $m^{-1}K^{-1}$. At a saturation temperature of 50 ºC, the liquid/gas density ratio is 13.1, and thermal conductivity of the liquid is 59.7 mW $m^{-1}K^{-1}$. Two main reasons for the heat transfer coefficient to decrease as the saturation temperature increases are the decrease in the liquid/gas density ratio and the thermal conductivity of the liquid. And, the effects of saturation temperature show a little different in each mass flux condition. In the case of mass flux of 400 kg m^{-2} s^{-1}, there are large differences relatively. On the other hand, in the case of mass flux of 100 kg m^{-2} s^{-1}, the differences are very small. The reason of this difference may be come from the measuring error.

4.1.4 Observation of two-phase flow regimes

Figure 5 shows the recorded images of two-phase flow patterns together with the measured heat transfer coefficients of HFO1234yf at a saturation temperature of 50 ºC. The value of vapor quality of the recorded images is from 0.9 to 0.1 about every 0.2. At a mass flux of 100 kg m^{-2} s^{-1}, the wavy flow was prevalent over most of the vapor quality range. At a low vapor quality, the heat transfer coefficients increase slightly with increasing vapor quality, especially at end of part due to the heat transfer is dominated mainly by intermediate flow region and gravity-dominated flow regime.

For a mass flux of 200 kg m^{-2} s^{-1}, approximately half of the vapor quality range is occupied by annular flow regimes. The heat transfer coefficients increase gradually with increasing vapor quality. The heat transfer is dominated by shear-dominated flow regime at the beginning of condensing, and then, fall into intermediate flow region, at latter part of vapor quality, is entirely gravity-dominated flow regime.

At mass fluxes ranging bwteen 300 kg m^{-2} s^{-1} and 400 kg m^{-2} s^{-1}, annular flow was prevalent over most of the vapor quality range. There is a clear dependency of the heat transfer coefficient on the vapor quality and the mass flux. As the vapor quality increases, the heat transfer coefficient also increases. The heat transfer is primarily in the shear-dominated flow regimes.

4.2 Effects of refrigerants properties on the heat transfer coefficient

The measured heat transfer coefficients of HFO1234yf were compared to those of R134a and R32 to analyze the effect of the thermal physical properties of the refrigerants on the heat transfer coefficient.

Comparisons of refrigerant properties at a saturation temperature of 40 ºC are listed in Table2. The primary thermal-physical properties that influence the heat transfer coefficient are the density and viscosity of liquid and vapor, and their ratio, together with the thermal conductivity.

Figure 6 shows the tendency of the heat transfer coefficient and the differences between the three refrigerants. R32 has the highest heat transfer coefficients. While the heat transfer coefficients of HFO1234yf are a little lower than that of R134a at the same condition because the thermal-physical properties of HFO1234yf (density ratio, viscosity ratio of liquid and vapor, the thermal conductivity) are all a little lower than that of R134a. The largest difference of heat transfer coefficient between HFO1234yf and R134a is 23.8% at mass flux of 100 kg m^{-2} s^{-1}.

4.3 Comparison with correlations

4.3.1 Comparison with flow regime maps

The flow regime map proposed by Tandon et al (1982) is used in this research and compared with the flow pattern of HFO1234yf in 4mm tube observed. The map uses the dimensionless vapor superficial velocity j^*_g and parameter (1-α)/α as coordinates expressed as follows. Table 3 shows the flow regimes and parameter ranges.

$$j_g^* = Gx / \left[gD\rho_g \Delta\rho \right]^{1/2} \tag{5}$$

$$\alpha = \left\{ 1 + \left(\rho_g / \rho_L \right) \left(\frac{1-x}{x} \right) \left[0.4 + 0.6 \sqrt{\frac{\frac{\rho_L}{\rho_g} + 0.4\left(\frac{1-x}{x} \right)}{1 + 0.4\left(\frac{1-x}{x} \right)}} \right] \right\}^{-1} \tag{6}$$

Figure 7 shows the comparison between the observed flow pattern and the flow regime map proposed by Tandon et al. As shown in this figure, almost all the observed annular flow patterns, including annular-mist, annular, semi-annular, and wavy-annular, fall into annular and semi-annular flow regimes map proposed by Tandon. The results show that this flow regime map can predict annular flow reliably. For the wavy flow observed in this study, half of experimental data were plotted outside the boundary of the wavy flow regime map and fall into annular and semi-annular flow regimes. The experimental data values resulting in wavy-annular flow could be attributed to the observation deviation. Slug flow and plug flow patterns are rarely observed in the flow pattern obtained experimentally, in addition, these two flow patterns cannot be predicted accurately using this flow regime map. The flow patterns observed can be attributed to the difference in definitions of the various flow patterns existing, which is somewhat subjective, especially for intermittent flow.

4.3.2 Comparison with pressure drop correlations

Figure 8 shows the measured pressures drop compared with the predicted values using the Lockhart-Martinelli correlation, Huang correlation, Haraguchi correlatoin added acceleration pressure drop as a function of the vapor quality of HFO1234yf at mass fluxes ranging from 100 kg m^{-2} s^{-1} to 400 kg m^{-2} s^{-1}, at a saturation temperature of 45 ºC. Table 4 summarizes the Lockhart-Martinelli correlation, Huang correlation, and Haraguchi correlatoin. Both the measured and predicted results showed that the pressure

drop increases when the vapor quality increases because the velocity of the refrigerant increases with the increase in vapor quality, which leads to a larger pressure drop. Moreover, as the mass flux of the refrigerant increases, the pressure drop is also increased. The differences in the measured pressure drop and predicted values using the Lockhart-Martinelli correlation increase with an increase in the mass flux, and the average deviation between the predicted value and measured results were about 29.8%. For the Huang correlation, the average deviation between the predicted value and measured results was about 38.2%. When using the Haraguchi model, the average deviation between the predicted value and measured results was about 27.3% while 62.5% of the data were predicted within ±30%.

4.3.3 Comparison with heat transfer correlations

Several correlations were selected in order to compare the experimental results of the heat transfer coefficient of the three refrigerants, as shown in Fig. 10. Totally 330 experimental data points were used. The correlations being compared includes the Shah correlation, the Cavallini correlation, the Dobson and Chato correlation, and the Haraguchi correlation, as summarized in Table 5. Table 6 shows the mean deviation and accuracy of the four correlations for the condensation heat transfer coefficient. Figure 9(a) shows the comparison of the Shah correlation with the experimental data. Because the Shah correlation was developed only for the annular flow regime, it had a relatively large deviation at a low mass flux of 100 kg m^{-2} s^{-1}. Apart from the mass flux of 100 kg m^{-2} s^{-1}, the mean deviation is 12.9%. This shows that the Shah correlation is acceptable for annular flow. At small mass flows, most of the regimes are gravity dominated flow. The Shah correlation generally underpredicted the heat transfer coefficient. In Figure 9(b) the predicted results of the Cavallini correlation were compared with experimental results. Although this correlation is supposed to be applicable for any flow patterns, we found that the mean deviation between the experimental data and the predicted values is 23.2%. Although the scatter is much smaller than that of Shah correlation, the Cavallini correlation was found to somewhat underpredict the experimental data.

Figure 9(c) and Figure 9(d) show relatively better comparison results with the experimental data using correlations of Dobson and Chato and that of Haraguchi. The application range of both the correlations can cover all the flow regimes of condensation. The correlation of Dobson and Chato predicts the experimental data well with a mean deviation of 14.8%. About 78% of the data were predicted within ±20%. The prediction of the Haraguchi correlation agrees fairly well with the experimental data, with a mean deviation of 10.8%. Nearly all the data were predicted within ±20%. Compared to the other three correlations, Haraguchi correlation gave the best prediction results. Figure 10 shows the comparison of the measured and predicted heat transfer coefficient of HFO1234yf against the vapor quality at different mass fluxes, at saturation temperatures of 40 ºC and 50 ºC. Comparison results show that the Haraguchi correlation can predict the condensation heat transfer coefficient of HFO1234yf at wide experimental conditions with reasonable accuracy.

5. Conclusions

The condensation experiments were carried out in a horizontal tube with an inner diameter of 4 mm at mass fluxes ranging from 100 kg m^{-2} s^{-1} to 400 kg m^{-2} s^{-1} and saturation temperatures of 40 ºC, 45 ºC, and 50 ºC using HFO1234yf, R134a, and R32 as the working fluid. The main conclusions of this research are as

follows:

1. The effects of mass flux and vapor quality on the heat transfer coefficient are primarily observed in the shear-force dominated flow regimes when the mass flux is high or the vapor quality is high.
2. The effects of thermophysical properties on the heat transfer coefficient at different saturations temperature using different refrigerants were analyzed. The results show that the thermal conductivity, density ratio and viscosity ratio play an important role in the variation of the heat transfer coefficient.
3. Flow patterns were also observed to help in the analysis of the changing tendency of the heat transfer coefficient, and the tendencies were compared with the flow pattern map. The flow pattern map proposed by Tandon et al (1982) could predict the annular flow well.
4. The Haraguchi correlation for predicting the local frictional pressure drop can predict the measured pressure drop best compared to the Lockhart-Martinelli correlation and Huang correlation.
5. The experimental heat transfer coefficient was compared with four heat transfer coefficient correlations. The results showed that the Haraguchi correlation agrees reasonably with the experimental data values, with a mean deviation of 10.8%.

Nomenclature

C	constant in Lockhart-Martinelli correlation
c_p	specific heat capacity, J kg^{-1} K^{-1}
d	inner diameter of tube, mm
d_o	outer diameter of tube, mm
f	fanning friction factor
Fr	Froude number
Fr^*	modified Froude number
g	acceleration of gravity, m s^{-2}
G	mass flux, kg m^{-2}s^{-1}
Ga	Galileo number $= \frac{g\rho_l(\rho_l-\rho_g)d^3}{\mu_l^2}$
$h_{\exp}$	experimental condensation heat transfer coefficient, kW m^{-2} K^{-1}
h_{lg}	latent heat, kJ kg^{-1}
j^*_g	dimensionless vapor superficial velocity
Ja	Jakob number $= \frac{c_p(T_{sat}-T_w)}{h_{lg}}$
J_G	$= xG/\left[gD\rho_g(\rho_l-\rho_g)\right]^{0.5}$
J_G^T	transition dimensionless gas velocity
l	length of test section, m

m_w mass flow rate of water, kg s^{-1}

Nu Nusselt number

p pressure, kPa

P_r reduced pressure

Pr Prandtl number

q heat flux, kW m^{-2}

Q heat exchange rate, kW

Re Reynolds number

$$\mathrm{Re}_{l0}=\frac{Gd}{\mu_l},\quad \mathrm{Re}_{g0}=\frac{Gd}{\mu_g}\quad \mathrm{Re}_l=\frac{G(1-x)d}{\mu_l},\quad \mathrm{Re}_g=\frac{Gxd}{\mu_g}$$

T_{in} inlet temperature, K

T_{out} outlet temperature, K

T_s saturation temperature, K

T_{wall} inside-wall temperature, K

T_{wo} outer wall temperature, K

ΔT (T_s-T_{wall}), ºC

x vapor quality

X_{tt} Lockhart-Martinelli parameter $=\left(\frac{1-x}{x}\right)^{0.9}\left(\frac{\rho_g}{\rho_l}\right)^{0.5}\left(\frac{\mu_l}{\mu_g}\right)^{0.1}$

z coordinate along the tube direction, m

Greek symbols

α void fraction

θ_l angle subtended from the top of tube to the liquid level

λ thermal conductivity, W m^{-1} K^{-1}

μ viscosity, Pa·s

ρ density, kg m^{-3}

σ surface tension, N m^{-1}

Φ_V two-phase flow multiplier for frictional pressure drop $=1+0.5\left[\frac{G}{\sqrt{gd\rho_g\left(\rho_l-\rho_g\right)}}\right]^{0.75}X_{tt}^{0.35}$

Subscripts

a ΔT independent flow regime

B free convection

d ΔT dependent flow regime

f frictional

F forced convection

g saturated vapor

g0	all mixture assumed to be gas
h	homogeous
l0	all mixture assumed to be liquid
l,L	liquid phase
sat	saturation
stra	fully stratified flow regime

Acknowledgements

This study was sponsored by the New Energy and Industrial Technology Development Organization, Japan, for the project titled “Development of Non-fluorinated Energy-Saving Refrigeration and Air Conditioning Systems. ”

References

Barbara, M.,Mark, S.,2008. HFO-1234yf Low GWP Refrigerant Update, International Refrigeration and Air Conditioning Conference

SAE, 2009, Industry evaluation of low global warming potential refrigerant HFO-1234yf, *SAE CRP-1234*, http://www.sae.org/standardsdev/tsb/cooperative/crp1234-3.pdf

Cavallini, A., Censi, G., Del Col, D., Doretti, L., Longo, G.A., Rossetto, L., 2003. Condensation inside and outside smooth and enhanced tubes: a review of recent research. Int. J. Refrigeration, 26, 373-392.

Cavallini, A., Censi, G., Del Col, D., Doretti, L., Matkovic, M., Rossetto, L., Zilio, C., 2006. Condensation in horizontal smooth tubes: a new heat transfer model for heat exchanger design. Heat Transfer Eng. 27, 31-38.

Cavallini, A., Censi, G., Del Col, D., Doretti, L., Longo, G.A., Rossetto, L., 2001. Experimental investigation on condensation heat transfer and pressure drop of new HFC refrigerants(R134a, R125, R32, R410A,R326ea)in a horizontal smooth tube. Int. J. Refrigeration, 24, 73-87.

Chisholm, D., 1967. A theoretical basis for the Lockhart-Martinelli correlation for two-phase flow. Int. J. Heat Mass Transf. 10, 1767–1778.

Del Col, D., Torresin, D., Cavallini, A., 2010. Heat transfer and pressure drop during condensation of the low GWP refrigerant R1234yf. Int. J. Refrigeration, 33, 1307-1318.

Dobson, M. K., Chato, J. C., Hinde, D.K., Wang, S.P., 1994. Experimental evaluation of internal condensation of refrigerants R12 and R134a. ASHRAE Trans. 100, 744-754.

Dobson, M.K., Chato, J.C., 1998. Condensation in smooth horizontal tubes, Int. J. Heat Transf., 120, 193-213.

Dobson, M. K., 1994. Heat transfer and flow regimes during condensation in horizontal tubes. ACRC TR-57.

Friedel, L., 1979. Improved pressure drop correlations for horizontal and vertical two phase pipe flow. 3R Int., 18, 485-492.

Haraguchi, H., Koyama, S., Fujii, T., 1994. Condensation of refrigerants HCFC22, HFC134a and

HCFC123 in a horizontal smooth tube (1st Report, Proposals of Empirical Expressions for the Local Frictional Pressure drop). Transactions of the Japan Society of Mechanical Engineers 60, 2117-2124.

Haraguchi, H., Koyama, S., Fujii, T., 1994. Condensation of refrigerants HCFC22, HFC134a and HCFC123 in a horizontal smooth tube (2nd Report, Proposals of Empirical Expressions for Local Heat Transfer Coefficient). Transactions of the Japan Society of Mechanical Engineers 60, 2117-2124.

Huang, X.C., Ding, G.L., Hu, H.T., Zhu, Y., Gao, Y.F., Deng, B.D., 2010. Two-phase frictional pressure drop Characteristics of R410A-oil mixture flow condensation inside 4.18mm and 1.6mm I.D. horizontal smooth tubes, HVAC&R Research 16(4),453-470.

Lockhart, R.W., Martinelli, R.C., 1949. Proposed correlation of data for isothermal two-phase, two-component flow in a pipe. Chem. Eng. Prog., 45, 39-48.

Matkovic, M., Cavallini, A., Del Col, D., Rossetto, L., 2009. Experimental study on condensation heat transfer inside a single circular minichannel. Int. J. Heat and Mass Transf., 52, 2311-2323.

Ghiaasiaan, S.M., 2008. Two-Phase Flow, Boiling, and Condensation in Conventional and Miniature Systems. Cambridge University Press, Cambridge.

Saitoh, S., Dang, C., Nakamura, Y., Hihara, E., 2011. Boiling heat transfer of HFO-1234yf flowing in a smooth small-diameter horizontal tube. Int. J. Refrigeration. “in press”

Soliman, H.M., 1983. Correlation of mist-to-annular transition during condensation,. Can. J. Chem. Eng. 61, 178–182.

Soliman, H.M., 1986. The mist-annular transition during condensation and its influence on the heat transfer mechanism. Int. J. Multiphase Flow, 12, 277-288.

Soliman, H.M., Azer, N.Z., 1971. Flow patterns during condensation inside a horizontal tube. ASHRAE Trans. 77, 210-224.

Shah, M.M., 1978. A general correlation for heat transfer during film condensation insides pipes. Int. J. Heat Mass Transf., 22, 547-556.

Smith, S.L., 1969-1970. Void fractions in two-phase flow: a correlation based upon an equal velocity heat model. Proc. Inst. Mech. Eng., 184, 647-657.

Tandon, T.N., Varma, H.K., Gupta, G. P., 1982. A new flow regimes map for condensation inside horizontal tubes. Int. J. Heat Transf., 104, 763-768.

Thome, J.R., El Hajal, J., Cavallini, A., 2003. Condensation in horizontal tubes, part 2: new heat transfer model based on flow regimes. Int. J. Heat Mass Transf., 46, 3365-3378.

Traviss, D.P., Rohsenow, W.M., Baron, A.B., 1973. Forced convective condensation in tubes: a heat transfer correlation for condenser design. ASHRAE Trans., 79, 157-165.

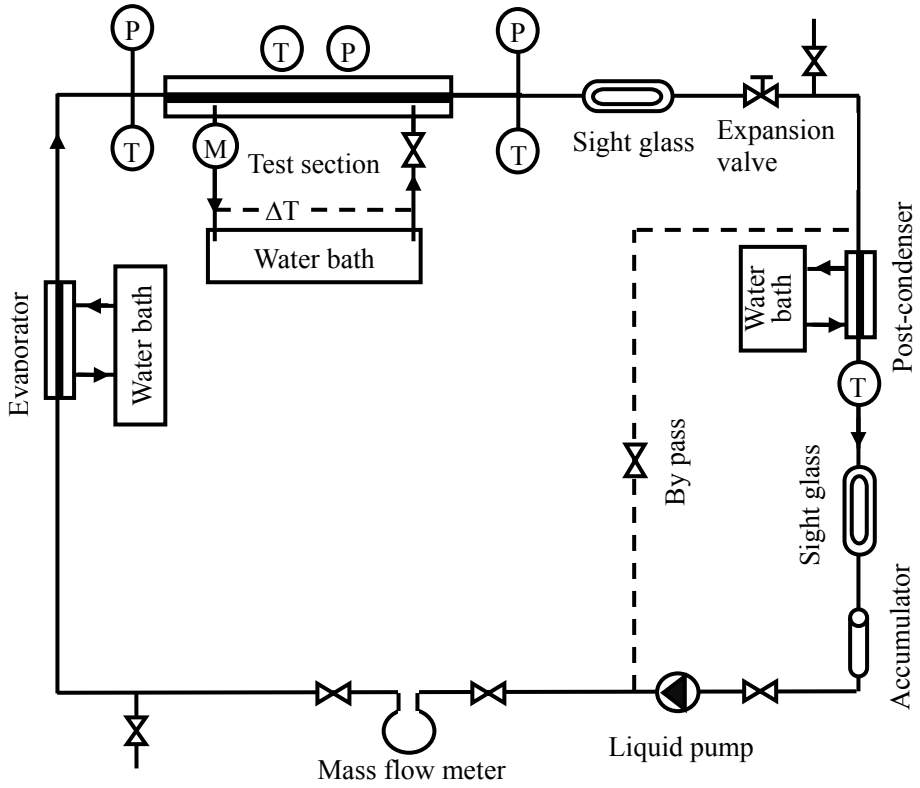

Figure 1. Schematic of the experimental apparatus

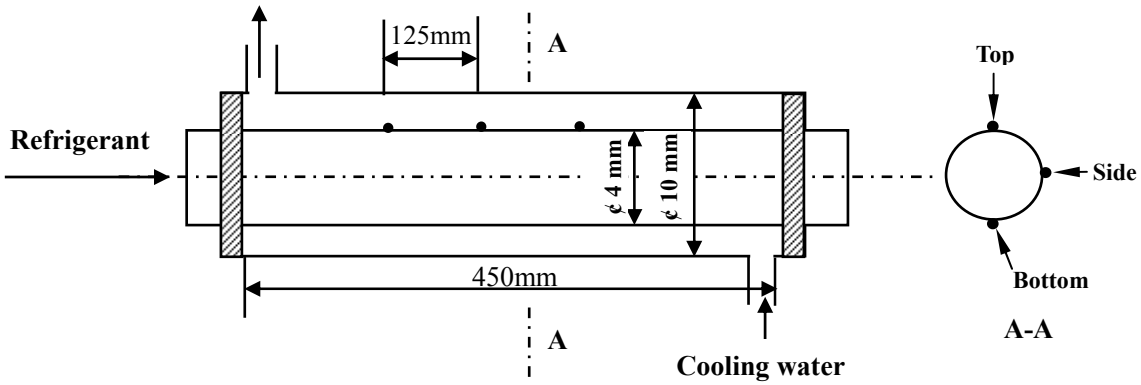

Figure 2. Detailed diagram of the test sub-sections

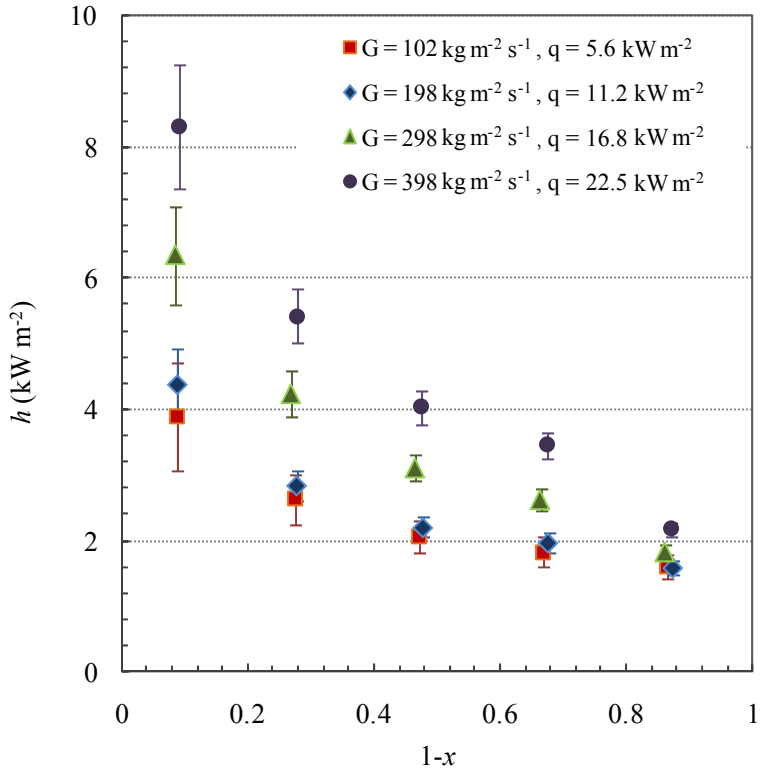

Figure 3. Effects of mass flux on the heat transfer coefficient of HFO1234yf at a saturation temperature of 45 ºC

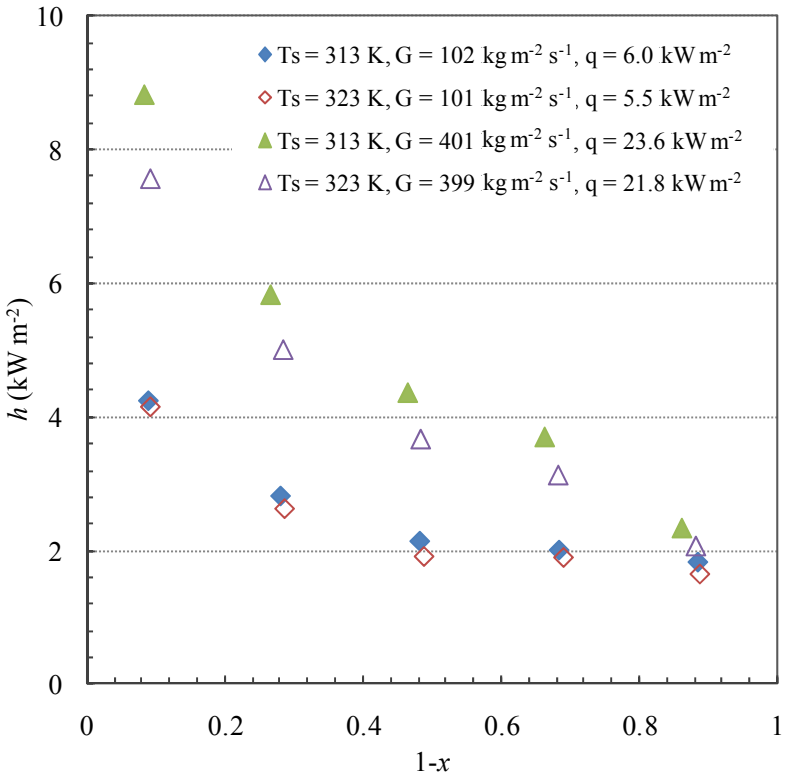

Figure 4. Effect of saturation temperatures at 40 ºC and 50 ºC on the heat transfer coefficient of HFO1234yf

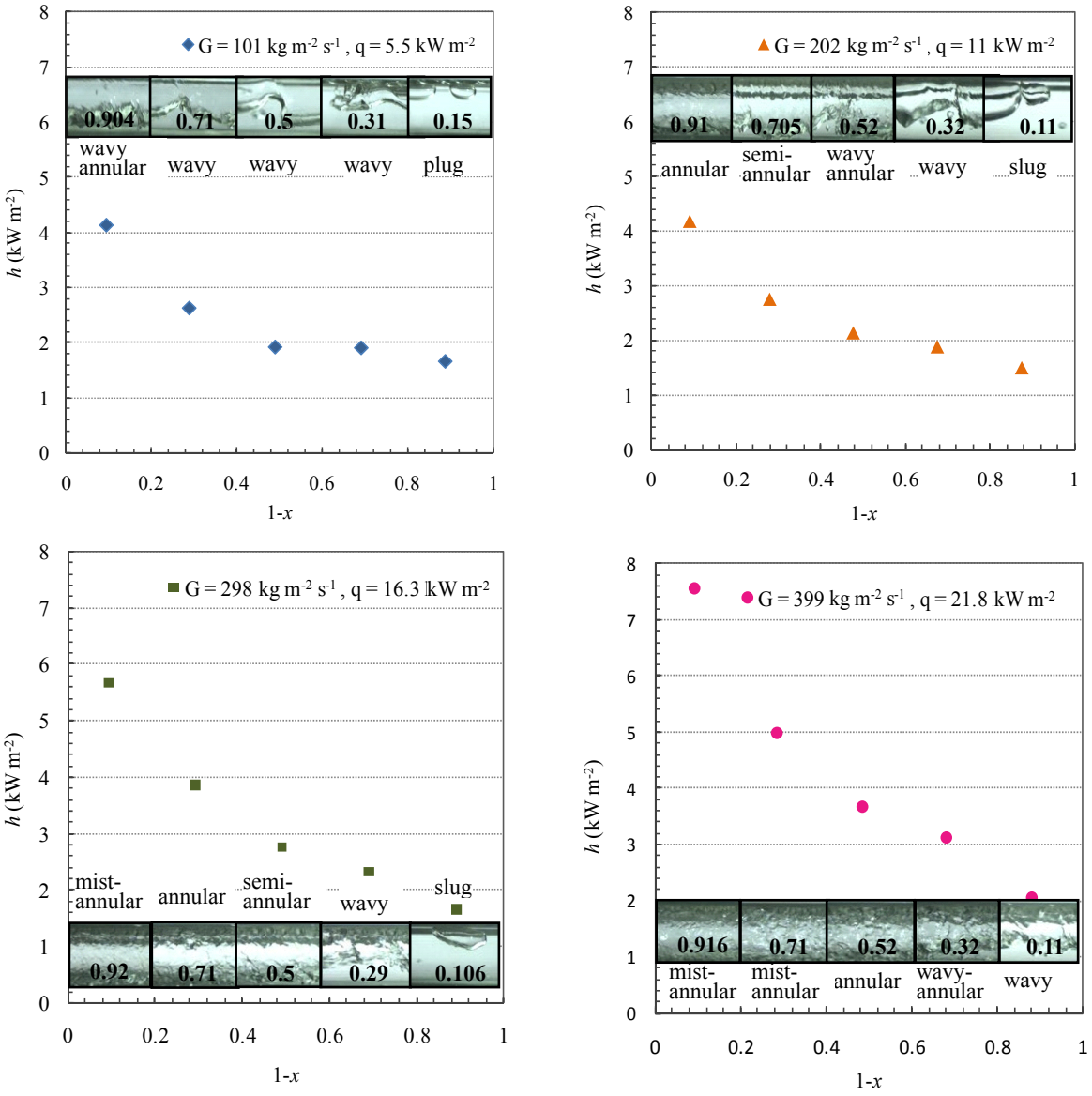

Figure 5. Observation of two-phase flow regimes of HFO1234yf at a saturation temperature of 50 ºC

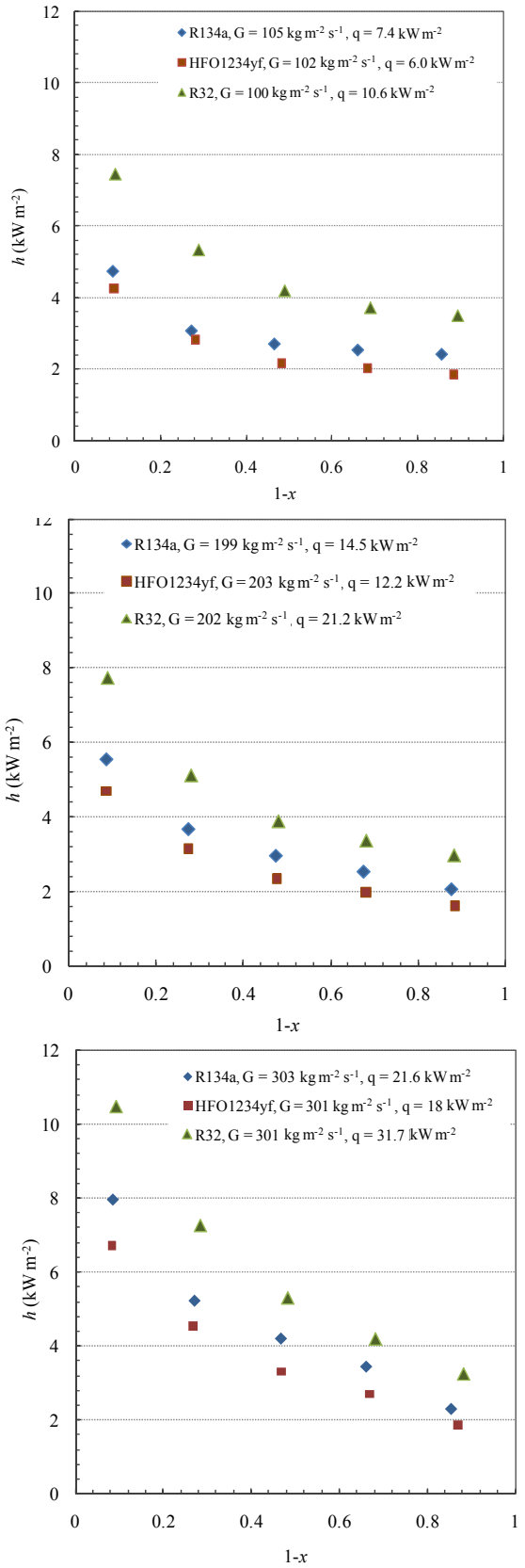

Figure 6. Heat transfer coefficient of R134a, HFO1234yf, and R32 at mass fluxes ranging from 100 kg m^{-2} s^{-1} to 300 kg m^{-2} s^{-1}

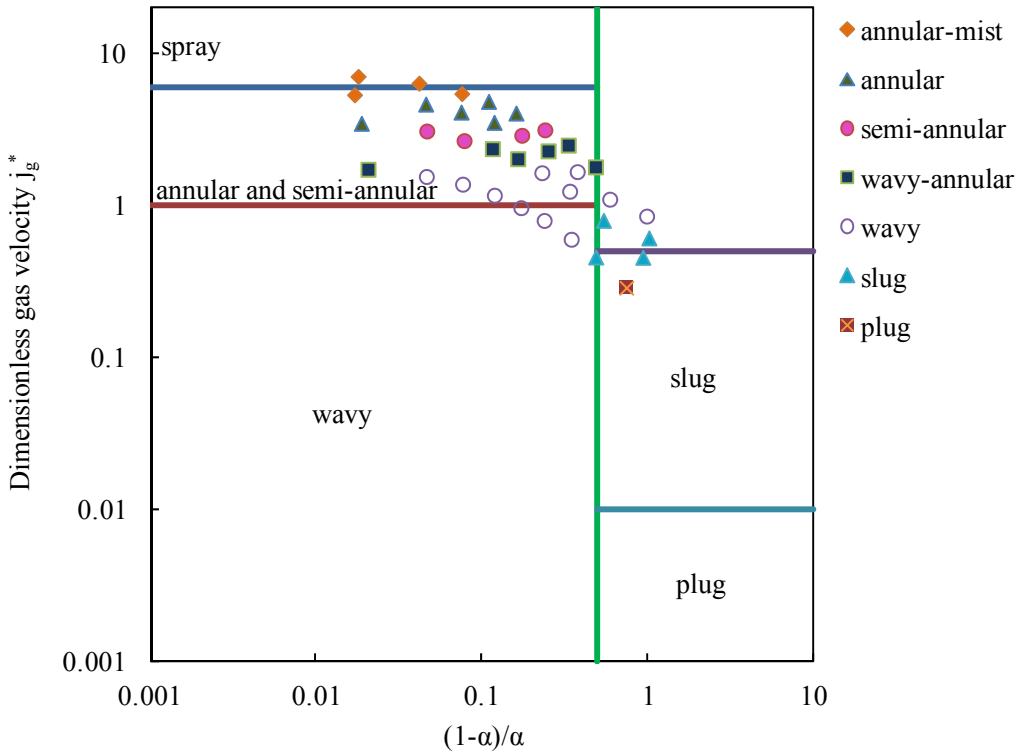

Figure 7. Comparison results of the observed flow pattern and flow regime map proposed by Tandon et al (1982)

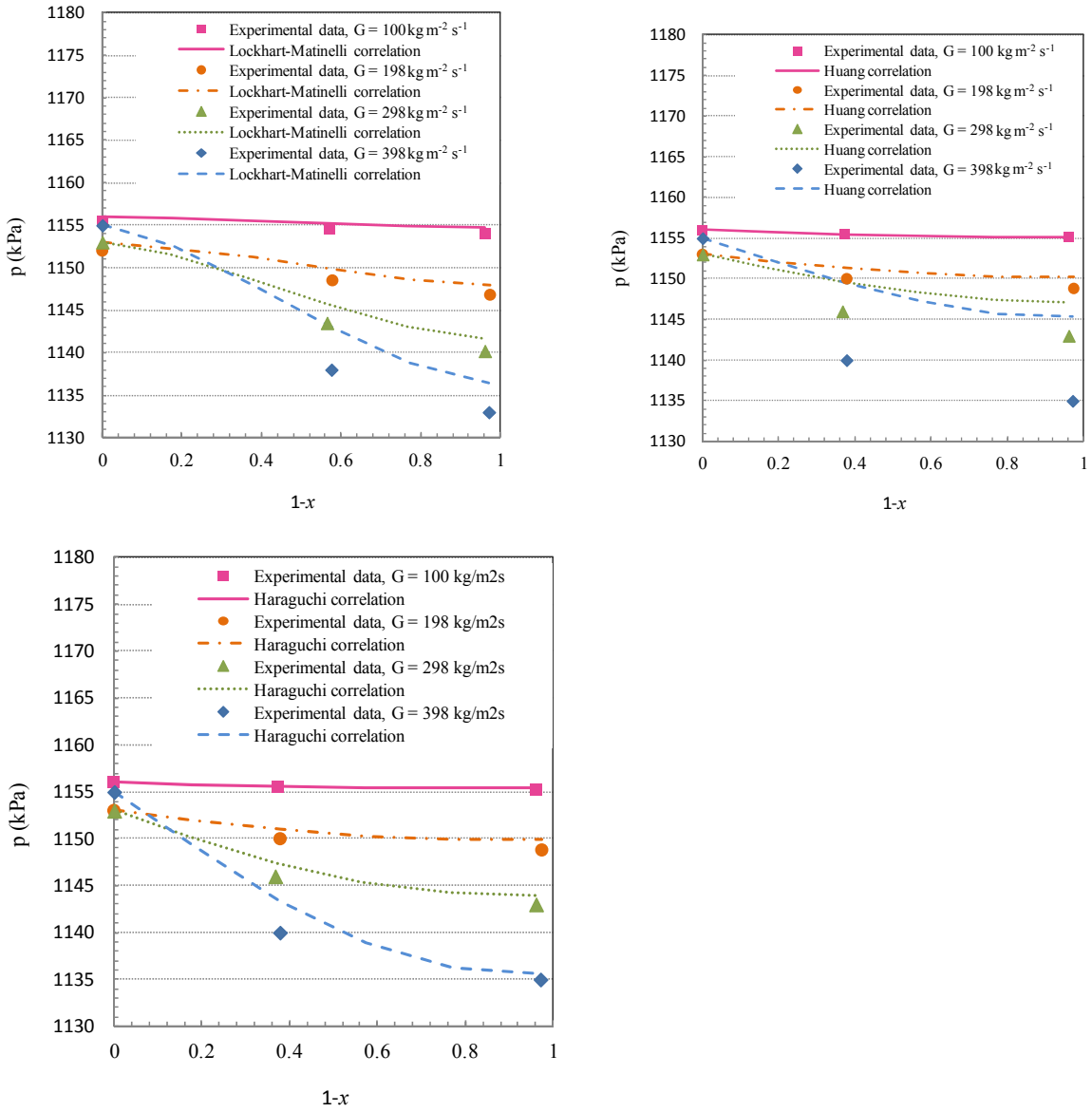

Figure 8. Comparison between the measured pressure drop and predicted values using the Lockhart - Martinelli correlation, Huang correlation, Haraguchi correlation and the acceleration pressure drop of HFO1234yf at mass fluxes ranging from 100 kg m^{-2} s^{-1} to 400 kg m^{-2} s^{-1} and a saturation temperature of 45 ºC

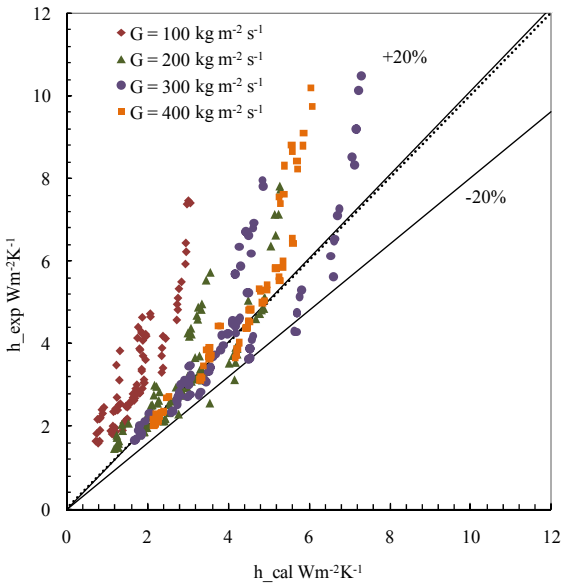

(a) Correlation of Shah

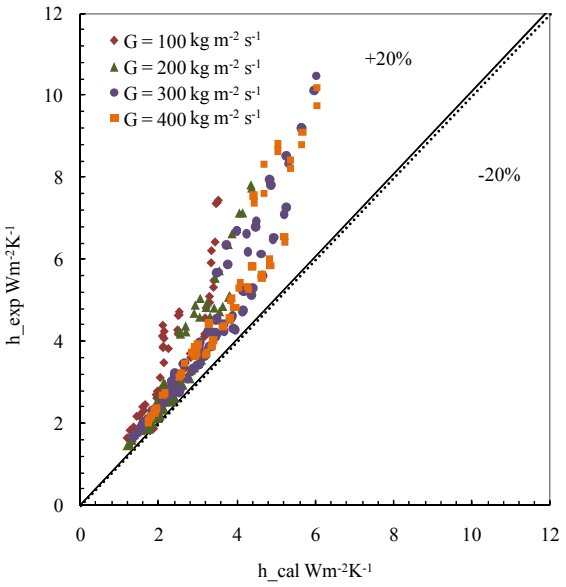

(b) Correlation of Cavallini

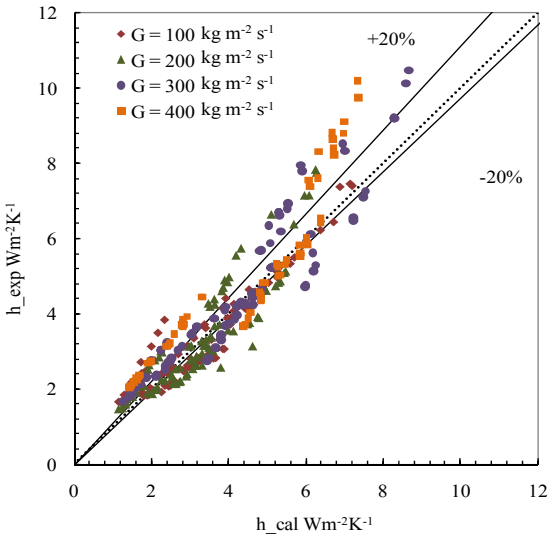

(c) Correlation of Dobson and Chato

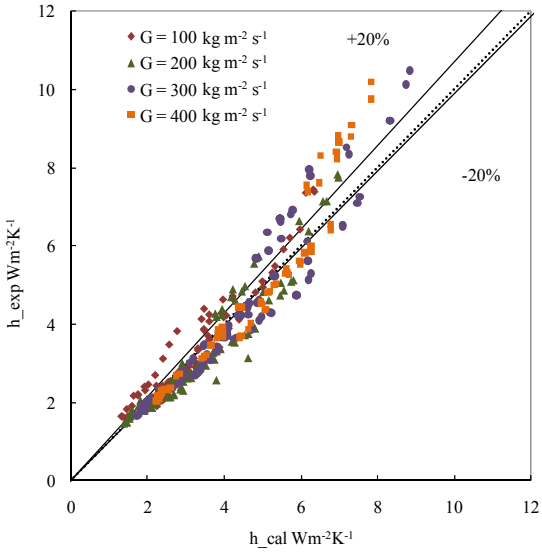

(d) Correlation of Haraguchi

Figure 9. Comparison between the measured and predicted heat transfer coefficient using the Shah, Cavallini, Dobson and Haraguchi correlation using HFO1234yf, R134a, and R32

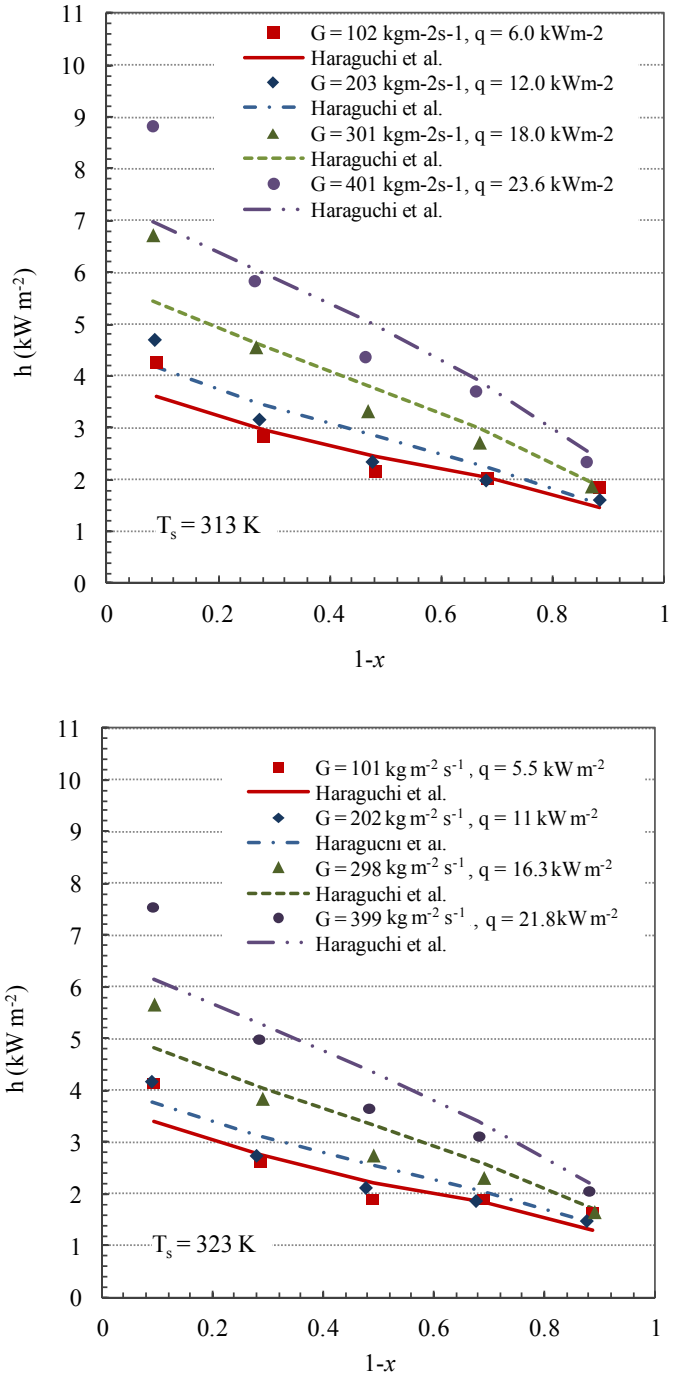

Figure 10. Comparison between the measured and predicted heat transfer coefficient using Haraguchi correlation with HFO1234yf at mass fluxes ranging from 100 kg m^{-2} s^{-1},and 400 kg m^{-2} s^{-1}, at saturation temperatures of 40 ºC and 50 ºC

Table 1. Properties of HFO1234yf at saturation temperatures of 40 ºC and 50 ºC

Properties of HFO1234yf	T_s = 313 K	T_s = 323 K
Pressure [Mpa]	1.018	1.302
Reduced pressure[-]	0.301	0.385
Liquid Density [kg m^{-3}]	1033.5	989.8
Vapor Density [kg m^{-3}]	57.7	75.7
Density Ratio[-]	17.9	13.1
Liquid Viscosity [g $cm^{-1}s^{-1}$]	0.00129	0.00115
Vapor Viscosity [g $cm^{-1}s^{-1}$]	0.000132	0.000139
Thermal Conductivity [mW $m^{-1}K^{-1}$]	62.98	59.73

Table 2. Comparison between the properties of R134a, HFO1234yf, and R32 at a saturation temperature of 40 ºC

Properties	HFO1234yf	R134a	R32
Pressure [Mpa]	1.018	1.017	2.478
Reduced pressure[-]	0.301	0.251	0.429
Liquid Density [kg m^{-3}]	1033.5	1146.7	893
Vapor Density [kg m^{-3}]	57.7	50.09	73.3
Density Ratio[-]	17.9	22.9	12.2
Liquid Viscosity [kg $m^{-1}s^{-1}$]	0.00129	0.00161	0.000949
Vapor Viscosity [kg $m^{-1}s^{-1}$]	0.000132	0.000124	0.000138
Viscosity Ratio[-]	9.77	13.3	6.88
Thermal Conductivity [mW $m^{-1}K^{-1}$]	62.98	74.7	114.58

Table 3. The flow regimes and parameter ranges of the flow regime map proposed by Tandon et al (1982)

Spray flow: $j_g^* \geq 6$ and $\frac{1-\alpha}{\alpha} \leq 0.5$
Annular and Semi-annular flow: $1.0 < j_g^* \leq 6$ and $\frac{1-\alpha}{\alpha} \leq 0.5$
Wavy flow: $j_g^* \leq 1$ and $\frac{1-\alpha}{\alpha} \leq 0.5$
Slug flow: $0.01 < j_g^* \leq 0.5$ and $\frac{1-\alpha}{\alpha} \geq 0.5$
Plug flow: $j_g^* \leq 0.01$ and $\frac{1-\alpha}{\alpha} \geq 0.5$

Table 4. Correlations for pressure drop

Lockhart - Martinelli correlation for pressure drop：

$$-\left(\frac{dp}{dz}\right)=-\left(\frac{dp}{dz}\right)_{\mathrm{l}}\phi_{\mathrm{l}}^{2}=-\left(\frac{dp}{dz}\right)_{\mathrm{g}}\phi_{\mathrm{g}}^{2}$$

$$\phi_{\mathrm{l}}^{2}=1+C/X_{tt}+1/X_{tt}{}^{2}$$

$$\phi_{\mathrm{g}}^{2}=1+CX_{tt}+X_{tt}{}^{2}$$

$$X_{tt}{}^{2}=\left(-\frac{dp}{dz}\right)_{\mathrm{l}}/\left(-\frac{dp}{dz}\right)_{\mathrm{g}}$$

$$\left(-\frac{dp}{dz}\right)_{\mathrm{l}}=\frac{2f_{l}(G(1-x))^{2}}{d\rho_{l}},\ \left(-\frac{dp}{dz}\right)_{\mathrm{g}}=\frac{2f_{g}(Gx)^{2}}{d\rho_{g}}$$

$$\mathrm{Re}_{l}>2300,\ f_{l}=0.079\,\mathrm{Re}_{l}^{-0.25},\ \ \mathrm{Re}_{l}<2300,\ f_{l}=16/\mathrm{Re}_{l},$$

$$\mathrm{Re}_{g}>2300,\ f_{g}=0.079\,\mathrm{Re}_{g}^{-0.25},\ \ \mathrm{Re}_{g}<2300,\ f_{g}=16/\mathrm{Re}_{g},$$

turbulent – turbulent flow, $C=20$;

viscous – turbulent flow, $C=12$;

turbulent – viscous flow, $C=10$;

viscous – viscous flow, $C=5$

Huang correlation:

$$\Phi_{V}=1.0+1.777X_{tt}^{0.561}$$

$$f_{g}=0.046/\mathrm{Re}_{g}^{0.2}$$

$$\left(-\frac{\mathrm{dP}}{\mathrm{dz}}\right)_{f}=\Phi_{V}^{2}\frac{2f_{g}G^{2}x^{2}}{\rho_{g}d}$$

Haraguchi model：

$$\Phi_{V}==1+0.5\left[\frac{G}{\sqrt{gd\rho_{g}\left(\rho_{l}-\rho_{g}\right)}}\right]^{0.75}X_{tt}{}^{0.35}$$

$$f_{g}=0.046/\mathrm{Re}_{g}^{0.2}$$

$$\left(-\frac{\mathrm{dP}}{\mathrm{dz}}\right)_{f}=\Phi_{V}^{2}\frac{2f_{g}G^{2}x^{2}}{\rho_{g}d}$$

Table 5. Correlations for the condensation heat transfer

Shah ;

$$\frac{h}{h_{l0}} = (1-x)^{0.8} + \frac{3.8x^{0.76}(1-x)^{0.04}}{P_r^{0.38}}$$

$$h_{l0}d/\lambda_l = 0.023(Gd/\mu_l)^{0.8}\,\mathrm{Pr}_l^{0.4}$$

Cavallini et al.,;

$$J_G = xG/\left[gD\rho_g(\rho_l-\rho_g)\right]^{0.5}$$

$$J_G^T = \left\{\left[7.5/(4.3X_{tt}^{1.111}+1)\right]^{-3} + 2.6^{-3}\right\}^{-1/3}$$

ΔT independent flow regime $J_G > J_G^T$

$$h_a = h_{l0}\left[1+1.128x^{0.817}(\rho_l/\rho_g)^{0.3685}(\mu_l/\mu_g)^{0.2363}(1-\mu_g/\mu_l)^{2.144}\,\mathrm{Pr}_L^{-0.1}\right]$$

ΔT dependent flow regime $J_G \le J_G^T$

$$h_d = h_{stra} + \left[h_a(J_G^T/J_G)^{0.8} - h_{stra}\right](J_G/J_G^T)$$

$$h_{stra} = 0.725\left\{1+0.741\left[(1-x)/x\right]^{0.3321}\right\}^{-1} \times \left[\lambda_l^3\rho_l(\rho_l-\rho_g)gh_{lg}/(\mu_l D\Delta T)\right]^{0.25} + (1-x^{0.087})h_{l0}$$

Dobson and Chato ;

$$\mathrm{Fr}^* > 20(Annular flow): Nu = 0.023\,\mathrm{Re}_l^{0.8}\,\mathrm{Pr}_l^{0.4}\left(1+\frac{2.22}{X_{tt}^{0.89}}\right)$$

$$\mathrm{Fr}^* < 20: Nu = \frac{0.23\,\mathrm{Re}_{g0}^{0.12}}{1+1.1X_{tt}^{0.58}}\left(\frac{Ga\,\mathrm{Pr}_l}{\mathrm{Ja}_l}\right)^{1/4} + (1-\frac{\theta_l}{\pi})\left[0.0195\,\mathrm{Re}_l^{0.8}\,\mathrm{Pr}_l^{0.4}\sqrt{1.376+\frac{c_1}{X_{tt}^{c_2}}}\right]$$

$$\theta_l \approx \pi - \cos^{-1}(2\alpha-1)$$

$$\alpha = \left(1+\frac{(1-x)}{x}(\frac{\rho_g}{\rho_l})^{2/3}\right)^{-1}$$

$$Fr_{l0} = G^2/\rho_l^2 gD \le 0.7:$$

$$c_1 = 4.172 + 5.48Fr_{l0} - 1.564Fr_{l0}^2$$

$$c_2 = 1.733 - 0.169Fr_{l0}$$

$$Fr_{l0} > 0.7: c_1 = 7.242, c_2 = 1.655$$

$$\mathrm{Fr}^* = \begin{cases} 0.025\,\mathrm{Re}_l^{1.59}\left[\dfrac{1+1.09X_{tt}^{0.039}}{X_{tt}}\right]^{1.5}\dfrac{1}{\sqrt{Ga}} & for\ \mathrm{Re}_l \le 1250 \\ 1.26\,\mathrm{Re}_l^{1.04}\left[\dfrac{1+1.09X_{tt}^{0.039}}{X_{tt}}\right]^{1.5}\dfrac{1}{\sqrt{Ga}} & for\ \mathrm{Re}_l > 1250 \end{cases}$$

Haraguchi et al.,;

$$\mathrm{Nu} = \left(Nu_F{}^2 + Nu_B{}^2\right)^{1/2}$$

$$Nu_F = 0.0152\left(1+0.6\,\mathrm{Pr}_l^{0.8}\right)\left(\Phi_V/X_{tt}\right)\mathrm{Re}_l^{0.77}$$

$$Nu_B = 0.725H(\alpha)\left(\frac{Ga\,\mathrm{Pr}_l}{\mathrm{Ja}_l}\right)^{1/4}$$

$$H(\alpha) = \alpha + \left\{10\left[(1-\alpha)^{0.1}-1\right]+1.7\times10^{-4}\,\mathrm{Re}_{l0}\right\}\sqrt{\alpha}\left(1-\sqrt{\alpha}\right)$$

$$\alpha = \left[1+\frac{\rho_g}{\rho_l}\left(\frac{1-x}{x}\right)\left(0.4+0.6\sqrt{\frac{\dfrac{\rho_l}{\rho_g}+0.4\left(\dfrac{1-x}{x}\right)}{1+0.4\left(\dfrac{1-x}{x}\right)}}\right)\right]^{-1}$$

Table 6. Mean deviation and accuracy of the four correlations for the condensation heat transfer coefficient

Correlation	Mean deviation (%)	Accuracy defined as fraction of data within ±20% error(%)
Shah	21.4	54.5
Cavallini et al.,	23.2	53.3
Dobson and Chato	14.8	72.7
Haraguchi et al.,	10.8	90.6

$$Mean\ \ deviation = \frac{1}{n}\sum_{i=1}^{n}\frac{\left|h_{\exp,i} - h_{\mathrm{cal,i}}\right|}{h_{\exp,i}} \times 100\%$$